Supporting Information

Synthesis and Soft Crystal Structure-Induced Broad Emission in $(NH_3C_6H_{12}NH_3)InBr_5 \cdot 2H_2O$

Shuva Biswas,[a#] Arnab Mandal,[a#] Diptikanta Swain,[b] and Kanishka Biswas [a,*]

[a]New Chemistry Unit, International Centre for Materials Science and School of Advanced Materials, Jawaharlal Nehru Centre for Advanced Scientific Research (JNCASR), Jakkur P. O., Bangalore 560064, India.

[b]Institute of Chemical Technology-IndianOil Odisha Campus, Bhubaneswar 751013, India.

# S.B. and A.M. contributed equally.

*Corresponding author.

E-mail for correspondence: kanishka@jncasr.ac.in

Methods.

Chemicals and materials

Hydrobromic acid (HBr, 47 wt % in H_2O, Spectrochem), indium acetate [$In(OAc)_3$, Sigma-Aldrich], 1,5-diamiono-2-methylpentane ($NH_2C_6H_{12}NH_2$, 99%, Sigma-Aldrich) and n-hexane (SDFCL, 99%) were used without further purification.

Synthesis of $(NH_3C_6H_{12}NH_3)InBr_5 \cdot 2H_2O$

1 mmol $In(OAc)_3$ powder was dissolved in 2 mL of concentrated HBr solution under vigorous stirring at 60 °C for 15 min followed by the addition of 1 mmol 1,5-diamiono-2-methylpentane (5P1). The mixture was stirred at 110 °C for 30 min to obtain a colourless solution. After slow cooling, the colourless $(5P1)InBr_5.2H_2O$ crystals were obtained. The product was filtered by a Whatman filter paper and washed with hexane to remove residual acid.

Single crystal X-ray diffraction (SCXRD).

Single crystal data were collected in two different temperatures such as low temperature (127 K) and room temperature (296 K) from Bruker D8 Venture diffractometer equipped with a Photon detector and graphite monochromatic Mo K_α radiation (λ = 0.71073 Å, 50 kV, 1 mA). The raw data was collected, reduced and integrated using APEX III Software. The structure was solved using SHELXS and refined by using SHELXL included in the WinGXsuite.[S1-S3]

The degrees of distortion of the octahedra were calculated based on the following equations:[S4]

$$\lambda_{oct} = 1/6 \sum_{n=1}^{6} [\frac{d_n - d_0}{d_0}]^2 \qquad (S1)$$

$$\sigma^2 = 1/11 \sum_{n=0}^{12} (\theta_n - 90^\circ)^2 \quad (S2)$$

where d_0 represents the average bond distance, d_n denotes six individual bond distances and θ_n implies the bond angles.

Powder X-ray diffraction (PXRD)

Rigaku Smart Lab diffractometer was used to collect room temperature PXRD patterns using Cu Kα radiation (λ =1.5406 Å) with an accelerating voltage of 40 kV (current of 30 mA). For the phase transition study, the low temperature PXRD data were collected on a Bruker D8 Advance X-Ray diffractometer by using Cu K_α radiation (λ = 1.5406 Å) equipped with a PheniX Oxford closed cycle helium cryostat with a temperature stability of 0.1 K.

Optical spectroscopy

Diffuse reflectance measurements were carried out to estimate the optical band gap for solid samples in the range of 250–800 nm by using a Perkin-Elmer Lambda 900 UV/vis/near-IR spectrometer in the reflectance mode. By using the Kubelka–Munk equation, absorption (α/*S*) data were calculated from the reflectance data:[S5]

$$\frac{\alpha}{S} = \frac{(1-R)^2}{2R} \quad \text{(S3)}$$

where *R* is the reflectance and α and *S* are the absorption and scattering coefficients, respectively. The band gaps for the solid sample were derived from α/*S* vs energy (eV) plots.

Thermogravimetric analysis (TGA)

Thermogravimetric analysis was carried out using a 2 STAR TGA instrument, in which the samples were heated in N_2 atmosphere (40 mL min^{-1}) at a rate of 5 °C min^{-1} in the temperature range of 40 − 600 °C.

Field emission scanning electron microscopy (FESEM)

FESEM images in backscattered mode, SEM-EDAX colour mapping and EDS spectra mapping were acquired using Thermo Fisher (FEI) Apreo 2 S field emission scanning electron microscope (FESEM) using a T1 detector.

Raman spectroscopy

Raman spectroscopy measurements of the (5P1)$InBr_5 \cdot 2H_2O$ powder sample was carried out in the range of 50-300 $cm^{-1}$with a Renishaw spectrometer. The excitation wavelength of the laser was 532 nm.

X-ray photoelectron spectroscopy (XPS)

X-ray photoelectron spectroscopy (XPS) measurement for the (5P1)$InBr_5 \cdot 2H_2O$ sample was accomplished with a Thermo Scientific spectrometer using an Al-Kα (1.487 keV) X-ray monochromatic source with variable spot size possessing a relative composition detection better than 0.1%.

Photoluminescence spectroscopy

All PL and PL excitation characterizations of (5P1)$InBr_5 \cdot 2H_2O$solid samples were recorded on an Edinburgh FLS1000 spectrofluorometer coupled with pulsed Xenon microsecond flash-lamp. Temperature-dependent PL measurements ranging from 75 to 300 K were carried out by using a vacuum-closed cycle refrigerator cryostat.

The peak shift of the STE with temperature was explained with the following equation by consideration of the competing effect between thermal expansion (A_{TE}) and electron-phonon interactions (A_{EP}):[S6]

$$E(T) = E_0 + A_{TE}T + A_{EP}\left(\frac{2}{\exp\left[\frac{\hbar\omega}{k_B T}\right]-1} + 1\right) \qquad \text{(S4)}$$

where E_0 represents the unrenormalized bandgap, which is defined as $E_0 = E(0) - A_{EP}$ [E (0) = band gap at 0K]. A_{TE} and A_{EP} are the contributions for thermal expansion(TE) and electron phonon (EP) interactions, respectively.

Heat capacity measurement and data fitting

Temperature-dependent (2-300 K) heat capacity (C_p) of (5P1)$InBr_5 \cdot 2H_2O$ was measured using Dynacool, Quantum Design Physical Property Measurement System (PPMS).

To experimentally validate the presence of low-frequency optical phonons in (5P1)$InBr_5 \cdot 2H_2O$, low-temperature (2-30 K) heat capacity (C_p) data has been fitted using Debye-Einstein model (Equation S5):[S7]

$$\frac{C_p}{T} = \gamma + \beta T^2 + \sum_n \left(A_n \left(\theta_{E_n}\right)^2 . (T^2)^{-\frac{3}{2}} . \frac{e^{\frac{\theta_{E_n}}{T}}}{\left(e^{\frac{\theta_{E_n}}{T}} - 1\right)^2} \right) \qquad \text{(S5)}$$

Here, γ represents the Sommerfeld coefficient reflecting the electronic contributions of C_p. The second term, $\beta = B(12\pi^4 N_A \kappa_B/5)\ (\Theta_D)^{-3}$ denotes the contributions from the Debye lattice, whereas N_A, Θ_D and κ_B are Avogadro number, Debye temperature and Boltzmann constant respectively. $B = 1 - \sum_n A_n/3NR$, where R symbolizes the universal gas constant, and N is the number of atoms per formula unit. The third term in equation S5 comprised of the contribution from the independent localized Einstein oscillators contributing to the total heat capacity. A_n and Θ_{En} represent the pre-factor and the Einstein temperature respectively for the n^{th} Einstein mode.

Sound velocity measurement

The longitudinal (v_l) and transverse (v_t) sound velocities were measured on a disc-shaped sample by using an Epoch 650 Ultrasonic Flaw Detector (Olympus) instrument with a transducer frequency of 5 MHz.

The Poisson's ratio (v_p) is linked with the sound velocities by the following equation:[S8]

$$v_p = \frac{1-2\left(\frac{v_t}{v_l}\right)^2}{2-2\left(\frac{v_t}{v_l}\right)^2} \qquad \text{(S6)}$$

Grüneisen parameter (γ) was calculated using the following equation:[S8]

$$\gamma = \frac{3}{2} \cdot \frac{1+v_p}{2-3v_p} \qquad \text{(S7)}$$

The mean sound velocity (v_m) was calculated using the following formula:[S8]

$$v_m = \left(\frac{3}{v_l^{-3}+2v_t^{-3}}\right)^{\frac{1}{3}} \qquad \text{(S8)}$$

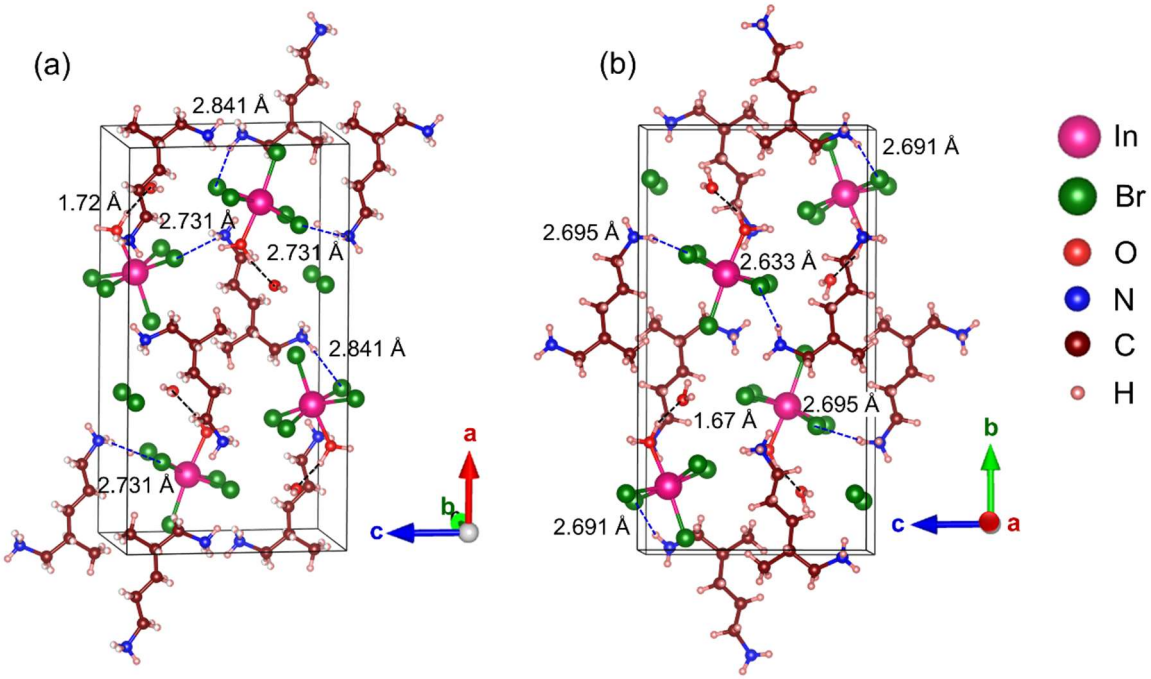

Fig. S1. Hydrogen bonding interactions in (5P1)$InBr_5 \cdot 2H_2O$, at (a) 296 K, (b) 127 K.

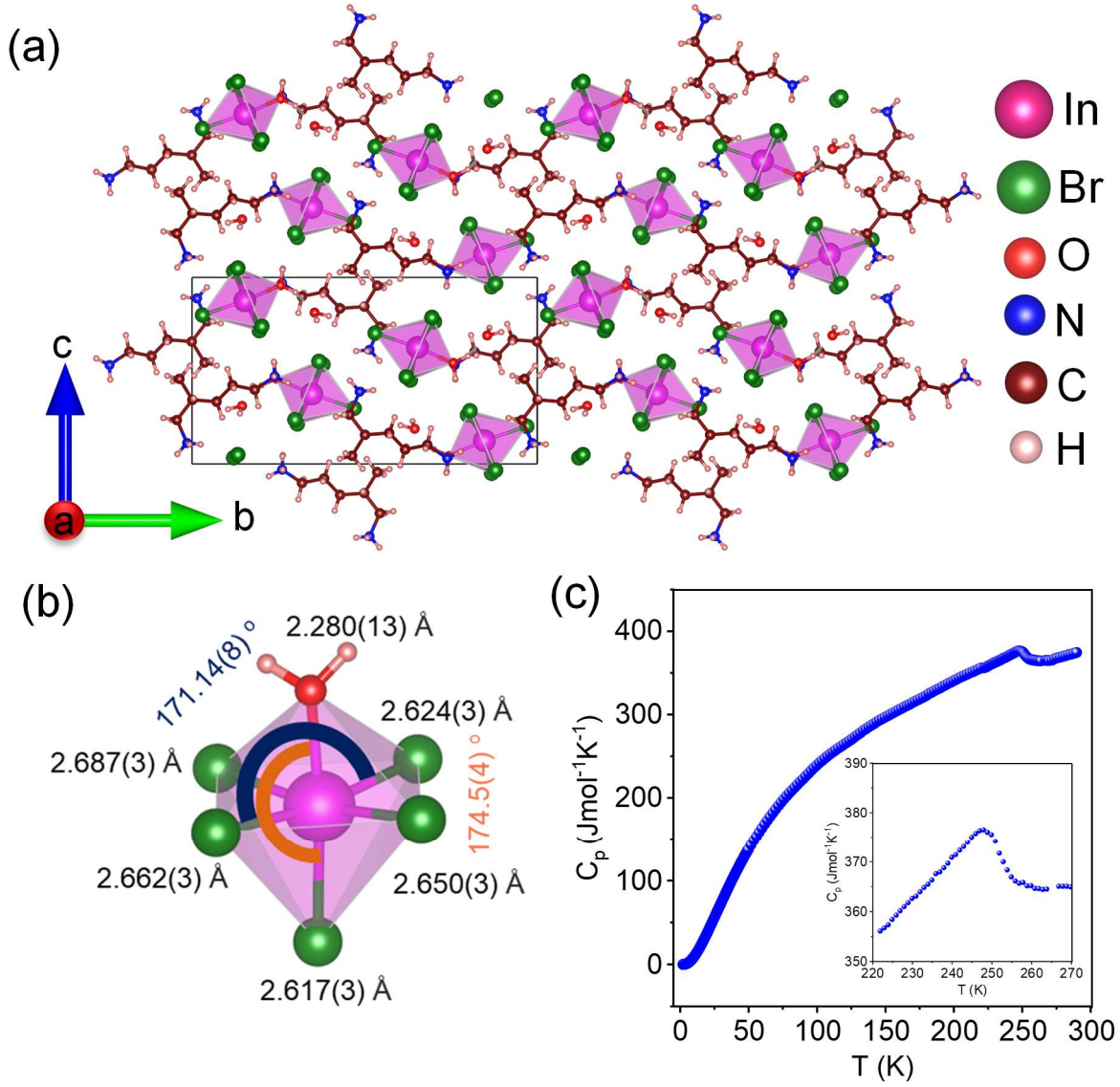

Fig. S2. (a) Low temperature (127 K) crystal structure of (5P1)$InBr_5 \cdot 2H_2O$ viewed along crystallographic *a*-axis. (b) Distorted $[InBr_5(H_2O)]^{2-}$ octahedron of (5P1)$InBr_5 \cdot 2H_2O$ at 127 K. (c) Temperature dependent C_p plot of (5P1)$InBr_5 \cdot 2H_2O$. Inset of (c) demonstrates the phase transition at 250 K.

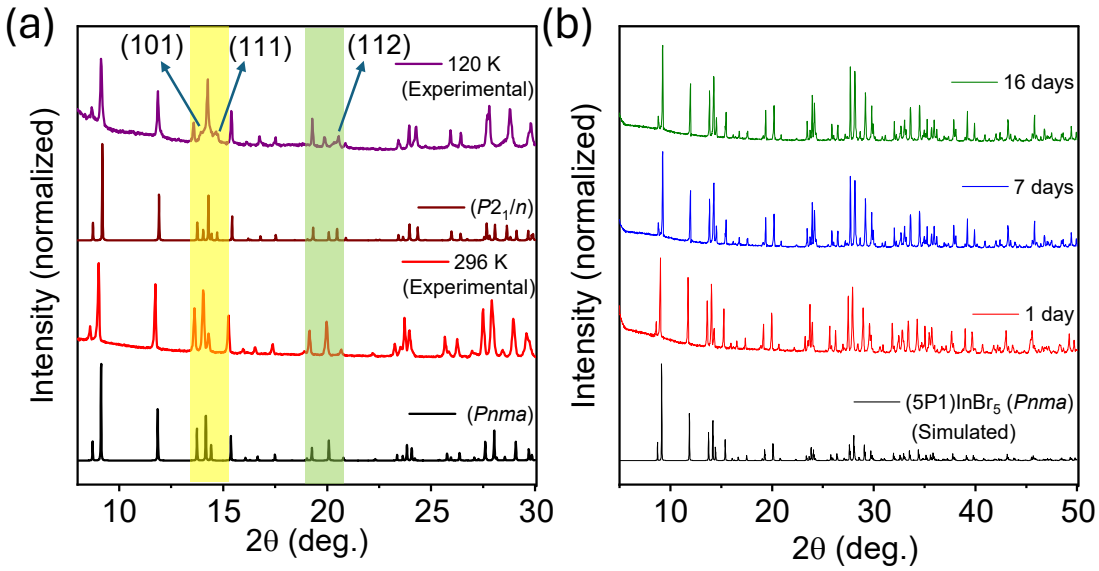

Fig. S3. (a) PXRD patterns at 120 K and 296 K of (5P1)$InBr_5 \cdot 2H_2O$ along with respective simulated patterns (yellow and green highlighted part indicate changes in PXRD patterns). (b) Comparison of PXRD patterns of as-synthesized (1 day) and aged (7 days and 16 days) (5P1)$InBr_5 \cdot 2H_2O$ sample.

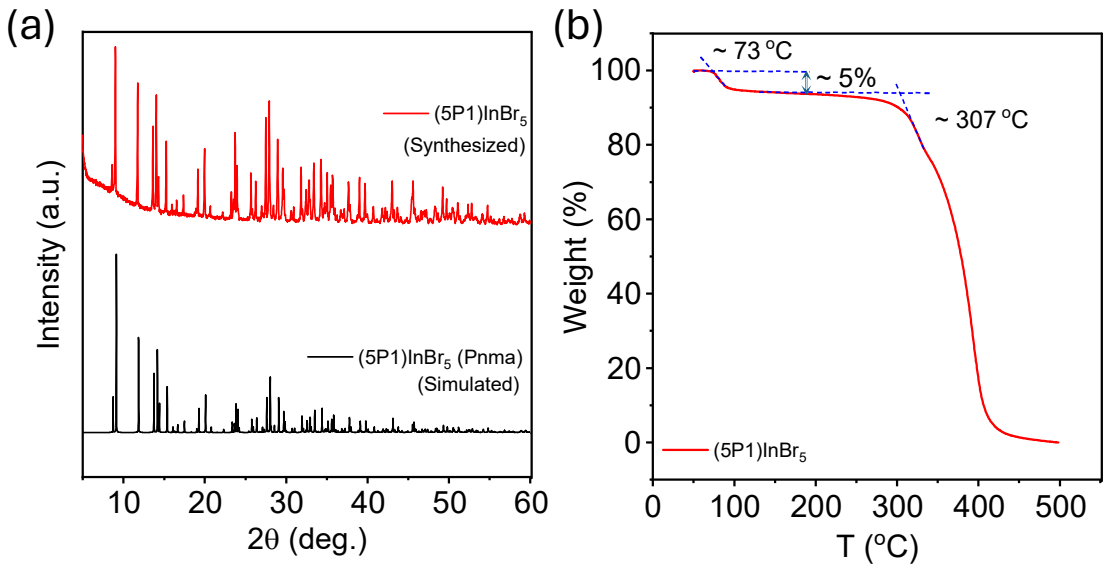

Fig. S4. (a) Comparison of PXRD patterns with the simulated patterns from SCXRD data for (5P1)$InBr_5 \cdot 2H_2O$ at 296 K. (b) TGA plot of (5P1)$InBr_5 \cdot 2H_2O$ showing 5 % weight loss due to loss of two water molecules.

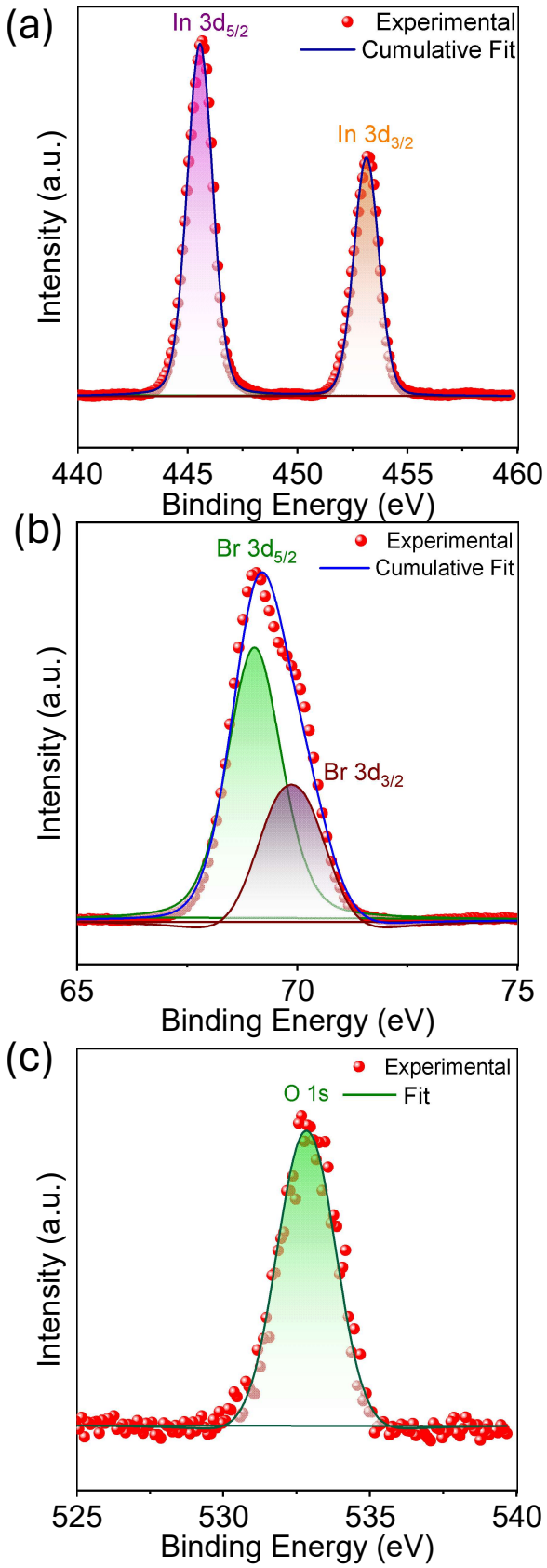

Fig. S5. XPS of (a) In *3d* (b) Br *3d* and (c) O *1s* levels in (5P1)$InBr_5 \cdot 2H_2O$ sample.

(a)

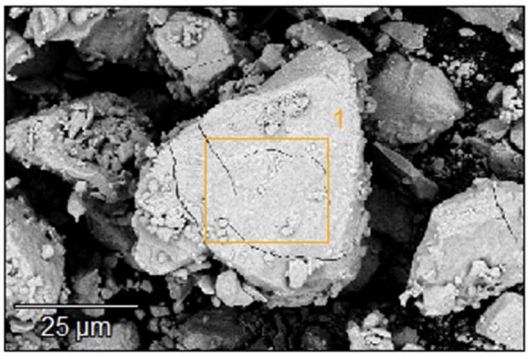

(b)

Element	Weight %	Atomic %
In	18.81	9.76
Br	73.70	54.96
C	4.93	24.45
N	2.42	10.31
O	0.14	0.52

(c)

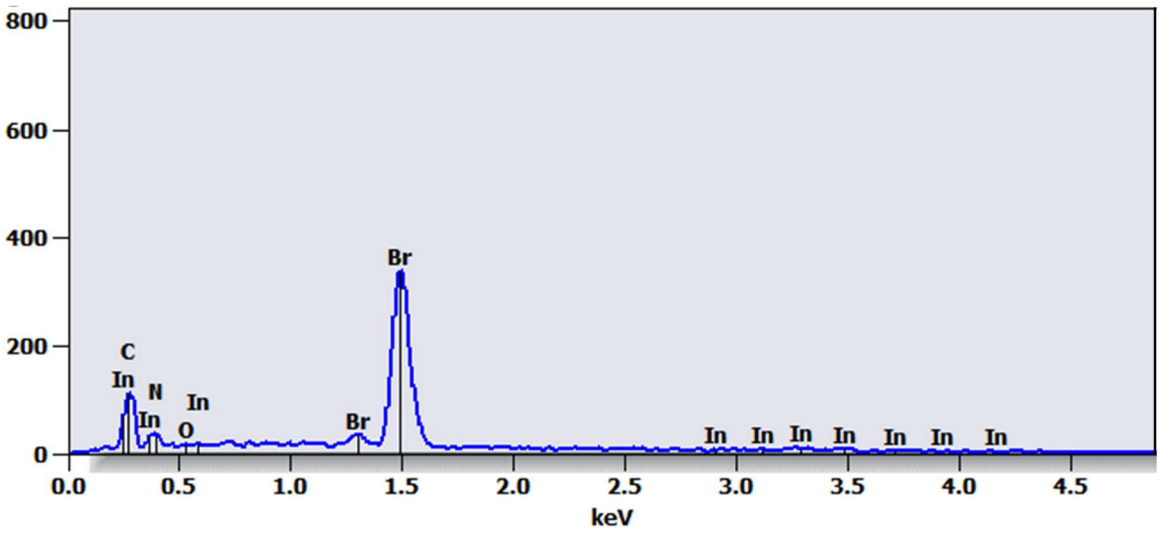

Fig. S6. (a) Backscattered FESEM image of (5P1)$InBr_5 \cdot 2H_2O$. (b) Weight and atomic percentage of In, Br, C, N, O atoms from the (c) EDX spectra of the marked area in (a) indicating Br/In ratio is ~5.63.

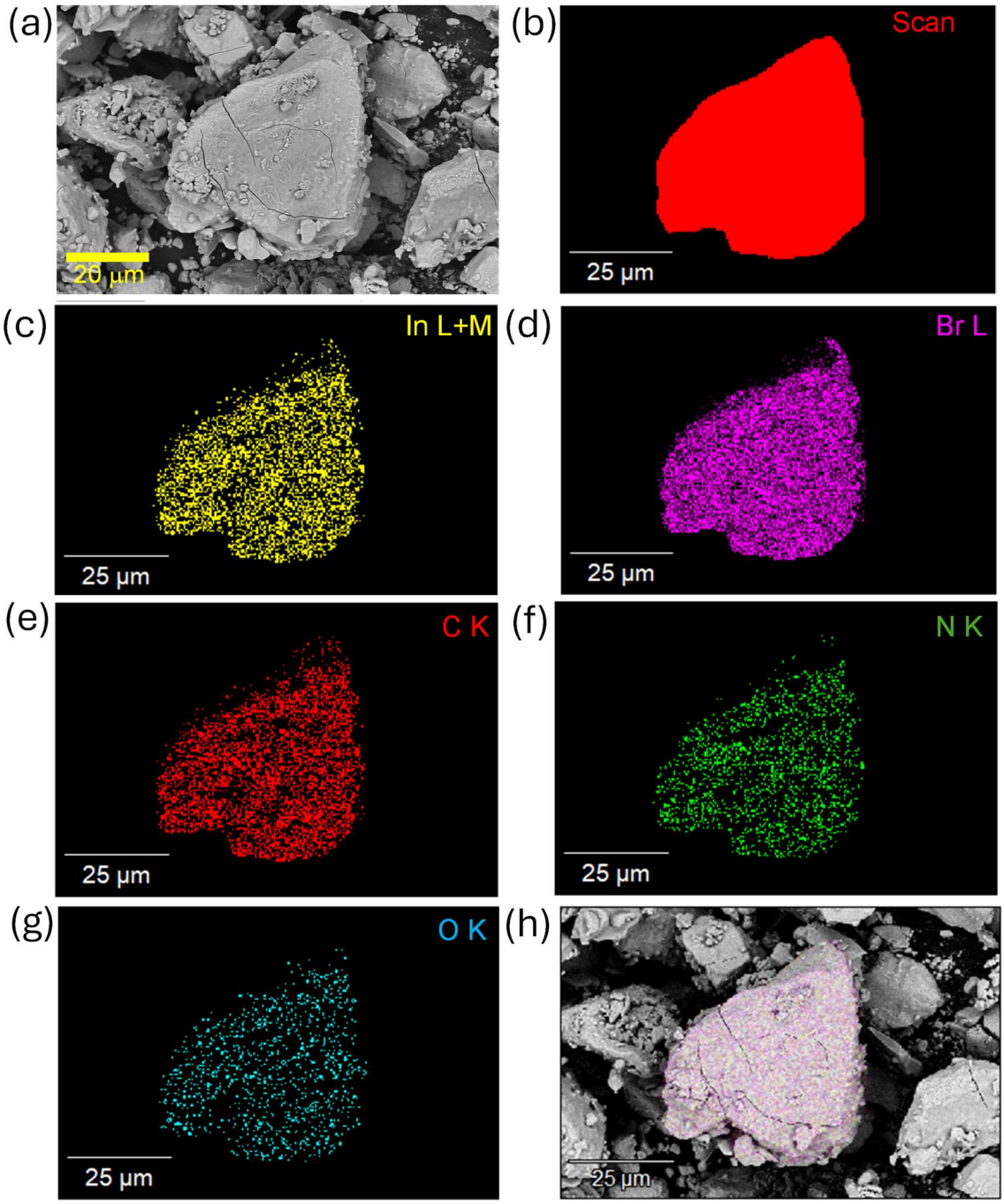

Fig. S7. (a) Backscattered FESEM image of grinded powder of (5P1)$InBr_5 \cdot 2H_2O$. (b) Scan area for EDAX mapping. EDAX colour mapping of (c) In L+M, (d) Br L, (e) C K, (f) N K, (g) O K and (h) overlapped mapping image showing homogeneous distribution of all the elements.

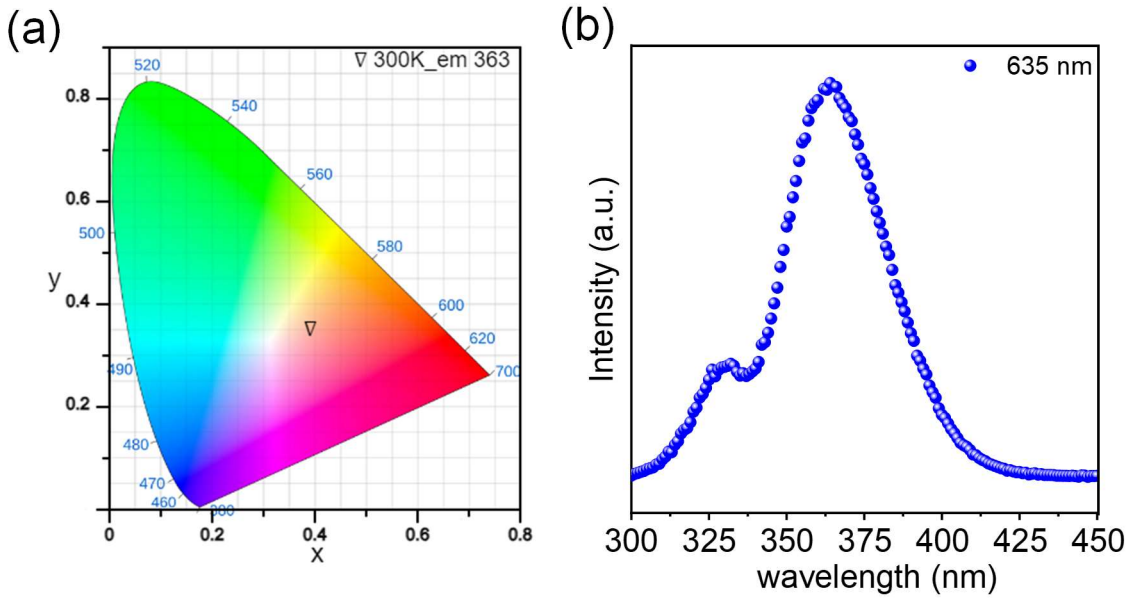

Fig. S8. (a) Chromaticity coordinate of (5P1)$InBr_5 \cdot 2H_2O$ plotted on the CIE1931 chromaticity chart. (b) Photoluminescence excitation (PLE) spectra of (5P1)$InBr_5 \cdot 2H_2O$ for STE emission.

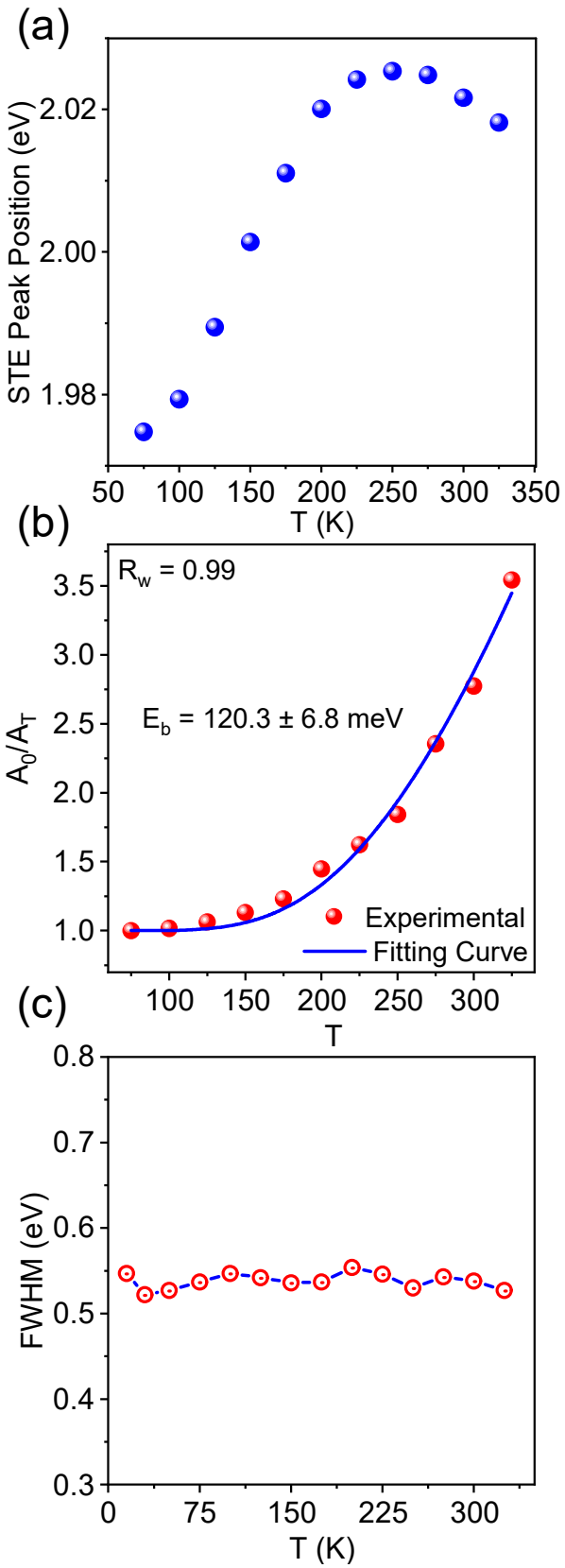

Fig. S9. (a) Variation of STE peak position (in eV) with temperature (b) Fitted plot of A_0/A_T vs T for calculation of exciton binding energy (E_b), (c) variation of FWHM of FE peak with temperature.

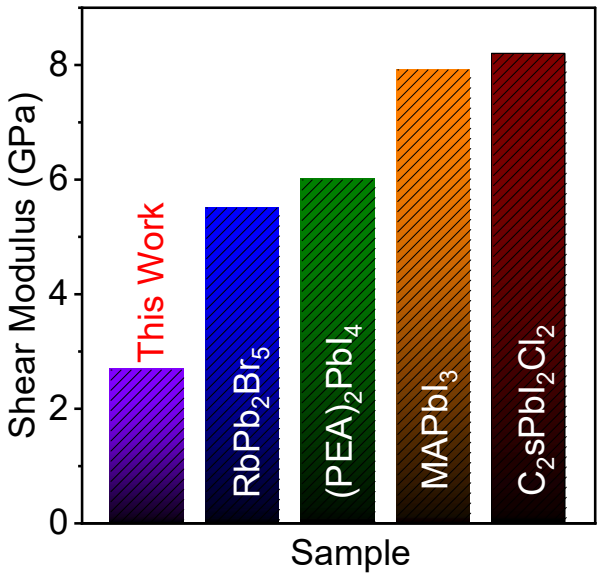

Fig. S10. Comparison of shear modulus (G) of (5P1)$InBr_5 \cdot 2H_2O$, with some of the other hybrid and all-inorganic metal halides like $RbPb_2Br_5$,[S9] $Cs_2PbI_2Cl_2$.[S10], $(PEA)_2PbI_4$,[S11] and $MAPbI_3$.[S11]

Table S1: Crystal structure data and refinement parameters from single crystal X-ray diffraction for (5P1)$InBr_5 \cdot 2H_2O$ (at 296 K) and LT-(5P1)$InBr_5 \cdot 2H_2O$ (at 127 K).

Empirical formula	**$C_6H_{18}N_2InBr_5 \cdot 2H_2O$**	**$C_6H_{18}N_2InBr_5 \cdot 2H_2O$**
Formula weight (g/mol)	668.62	668.62
Temperature (K)	296(2)	127(2)
Crystal system	Orthorhombic	Monoclinic
Space group	*Pnma*	*$P2_1/n$*
Unit cell dimensions		
a (Å)	20.264(3)	7.8333(13)
b (Å)	7.9353(11)	20.223(3)
c (Å)	11.0226(13)	10.9317(17)
α (°)	90	90
β (°)	90	91.232(7)
γ (°)	90	90
Volume ($Å^3$)	1772.4(4)	1731.3(5)
Z	4	4
Density (calc) (g/cm^3)	2.506	2.565
F(000)	1248	1248
θ range for data collection (°)	2.731-27.142	2.601-27.352
Index ranges	$-25 \le h \le 26$,	$-10 \le h \le 10$,
	$-10 \le k \le 10$,	$-25 \le k \le 25$,
	$-14 \le l \le 14$,	$-14 \le l \le 14$,
Reflections collected	62850	34407
Independent reflections	2102 [R_{int} = 0.0626]	3854 [R_{int} = 0.0803]
Completeness (%)	99.9	99.8
Refinement method	*full-matrix least-squares on F^2*	
Final R indices [I > 2σ(I)]	R_{obs} = 0.0304,	R_{obs} = 0.0856,
	wR_{obs} = 0.0839	wR_{obs} = 0.2492
Largest diff. peak and hole ($e \cdot Å^{-3}$)	1.23 and -1.67	3.70 and -1.39
GoF	1.040	1.078
CCDC no.	2348109	2348112

Table S2. Hydrogen bond distances for (5P1)$InBr_5 \cdot 2H_2O$ at 296 K and 127K.

Hydrogen bond (Å)	296 K	127 K
N-H···Br bond	2.731 Å 2.841 Å	2.633 Å 2.691 Å 2.695 Å
O-H···O bond	1.72 Å	1.67 Å

Table S3. Bond distortion level (λ_{oct}) and bond angle variance (σ^2) at different temperatures.

Material	λ_{oct}	σ^2
(5p1)$InBr_5$ (298 K)	2.68×10^{-3}	20.175
(5p1)$InBr_5$ (127 K)	2.89×10^{-3}	20.153

Table S4. Fitting parameters of low-temperature heat capacity according to Debye +3 Einstein modes.

Parameter	Value
γ ($Jmol^{-1}K^{-2}$)	0.034
β ($Jmol^{-1}K^{-4}$)	6.516×10^{-4}
Θ_{E1} (K)	23
Θ_{E2} (K)	49
Θ_{E3} (K)	99
Θ_D (K)	138

Table S5. Measured sound velocity and related parameters for (5P1)$InBr_5 \cdot 2H_2O$.

Parameter	Experimental value
Longitudinal sound velocity (m/s)	2237
Transverse sound velocity (m/s)	1035
Mean sound velocity (m/s)	1166
Poisson's ratio	0.36
Debye temperature (K)	146
Gruneisen parameter	2.25
Bulk modulus (GPa)	8.96
Shear modulus (GPa)	2.68

References:

S1. G. M. Sheldrick, *Acta. Cryst.*, 2008, **64**, 112-122.

S2. G. M. Sheldrick, *Acta. Cryst.* 2015, **71**, 3-8.

S3 L. J.Farrugia, *J.Appl. Cryst.*1999, **32**, 837-838.

S4. A. Mandal, S. Gupta, S. Dutta, S. K. Pati and S. Bhattacharyya, *Chem. Sci.*, 2023, **14**, 9770–9779.

S5. R. Pathak, D. Sarkar and K. Biswas, *Angew. Chem. Int. Ed.*, 2021, **60**, 17686-17692.

S6. B. Ai, C. Liu, Z. Deng, J. Wang, J. Han, X. Zhao, *Phys. Chem. Chem. Phys.* **2017**, *19*, 17349–17355.

S7. A. Bhui, S. Das, R. Arora, U. Bhat, P. Dutta, T. Ghosh, R. Pathak, R. Datta, U. V. Waghmare and K. Biswas, *J. Am. Chem. Soc.*, 2023, **145**, 25392-25400.

S8. R. Pathak, P. Dutta, A. Srivastava, D. Rawat, R. K. Gopal, A. K. Singh, A. Soni and K. Biswas, *Angew. Chem. Int. Ed.*, 2022, **61**, e202210783.

S9. J. Pradhan, A. Das, K. Kundu, Chahat and K. Biswas, *Chem. Sci.*, 2022, **13**, 9952-9959.

S10. P. Acharyya, T. Ghosh, K. Pal, K. Kundu, K. Singh Rana, J. Pandey, A. Soni, U. V. Waghmare and K. Biswas, *J. Am. Chem. Soc.*, 2020, **142**, 15595-15603.

S11. S. Rathore, W. L. Leong and A. Singh, *J. Alloys Compd.*, 2023, **936**, 168328.